

In-situ biological ozone detection by measuring electrochemical impedances of plant tissues

Serge Kernbach

CYBRES GmbH, Research Center of Advanced Robotics and Environmental Science,
Melunerstr. 40, 70569 Stuttgart, Germany, serge.kernbach@cybertronica.de

Abstract—This work demonstrates biological detection of a low concentration of O₃ by measuring electrochemical impedances of tissues in tobacco and tomato plants located indoor and outdoor. The lower range of generated ozone in the O₃-air mix is about 30 μgm⁻³ over the atmospheric level, which allows phytosensors to be considered as biodetectors of environmental pollutants. The ozone stress affects stomatal regulation that in turn influences the hydrodynamics of fluid transport system in plants. Sensors utilize electrochemical impedance spectroscopy (EIS) to measure ionic fluid content at several positions on the plant stem and calculate a variation of fluid distribution in control and experimental cases indoors. Outdoor setup uses the same methodology and sensors but different analysis due to uncontrolled nature of ozone pollution and the overlap of various stressors. The measurement results indicate a qualitative and quantitative reaction of hydrodynamic system to changes in O₃ concentration in the upper part of stem with a delay of 10-20 minutes between the onset of exposure and biological response. The probability of false-negative responses from a single plant is about 0.15±0.06. Pooling data from at least three plants allows for 92% confidence in detecting excess O₃. Measurements on days with low and high ozone levels of 80 μgm⁻³ to 130 μgm⁻³ result in a 2.33-fold difference in sensor values and thus demonstrate biological detection of high O₃ also outdoors. Statistically significant data include 948 sensor-plant attempts during 51 days with 9 plants and about 10⁷ samples collected in automated experiments. Long-term measurements have demonstrated the high reliability of electrochemical sensors, especially in harsh outdoor conditions with rain, heat and UV/IR radiations. The described approach has applications in environmental monitoring, biological pollution detection and biosensing; low-cost EIS sensors can be utilized in precise agriculture and vertical farming to detect nonspecific biotic and abiotic stressors.

Index Terms—Biosensors, sustainable biomonitoring, environmental pollution, low ozone concentration, electrochemical impedance spectroscopy

I. INTRODUCTION

O₃ is one of the major environmental pollutants [1], [2], it triggers various reactions in plant organisms [3], [4], affects stomatal regulation [5] and leads to different physiological changes [6]. Biological detection of ozone (as well as other environmental pollutants) can be conducted by measuring such physiological responses in-situ [7], [8]. It has already been demonstrated that high O₃ values (>1ppm) can be reliably detected by sensing electrophysiological parameters such as biopotentials and tissue impedances [9]. Focus on electrophysiological measurements is explained by their practical relevance, among others, the simplicity and reliability of sensors, enabling outdoor and field applications.

This work extends this approach for lower O₃ concentrations, following variations of surface atmospheric O₃ at 40-50 ppbv level [10], [11]. Since changes in stomata conductance induced by O₃ in turn alter hydrodynamic parameters of water-sap transport in the plant stem, we apply electrochemical impedance

spectroscopy (EIS) [12] to capture fluid dynamics in stem tissues. EIS has a number of applications in plant science [13], [14], allowing to record various physiological parameters [15]. In this work, differential EIS is used for two-point measurements – in the lower and upper regions of stem – representing different parameters of the fluid transportation system [16]. In addition, leaf transpiration and several environmental parameters are recorded.

For biosensing, we use tomato and tobacco plants, motivated by previous research and a high sensitivity of tobacco to O₃ stress [17], [18]. Tobacco has already been employed as a biosensor for O₃ monitoring [19]. The generation and sensing of low O₃ concentrations represents several technological issues. We utilize four O₃ sensors, high resolution data loggers, calibrations and a PWM-controlled O₃ generator to produce O₃-air mix with the required ozone concentration.

In addition, long-term measurements were performed under outdoor conditions with tomato plants during summer with high (120-149 μgm⁻³) and low (60-80 μgm⁻³) concentrations of atmospheric O₃. Outdoor setup is characterized by overlapping of several stressors (O₃, heat, NOx, PMx, UV/IR, mechanical impact) affecting plants from physiological level up to the level of physical chemistry [20]. The indoor setup allows isolating only O₃ stress, exploring different types of physiological reactions and performing a sufficient number of iterative experiments to collect statistically significant data.

All experiments were conducted automatically with continuous recording of all biological and environmental parameters and pre-programmed timing/PWM settings of generated O₃-air mix. Human intervention in both setups during 51 days of experiments was minimal. With two exposures per day and 6 plants, we accumulated data from about 768 indoor plant-sensor trials. The outdoor setup with 3 plants produced 180 measurement attempts. The described approach has several applications for environmental monitoring such as biological pollution detection, biosensing and biohybrid system development. Furthermore, low cost EIS sensors can be utilized in precise agriculture and vertical farming [16] for detecting different biotic and abiotic stressors or metabolic activities [21].

II. METHODS AND SETUP

Indoor setup. Measurements have been conducted in a measurement chamber shown in Figs. 1-3 with three tobacco (*Nicotiana tabacum*, var. *Habana*) and three tomato (*Solanum lycopersicum* 'Balkonzauberer') plants. Preparation of O₃-air mix with the required O₃ concentration is done in a 40L preparatory chamber with a low power O₃ generator (JB-OZ-S28 generator, 500mg/h in water part) and air pump (MT100, Air Cycle, diameter 100mm, 90 m³/h), see the scheme in Fig.

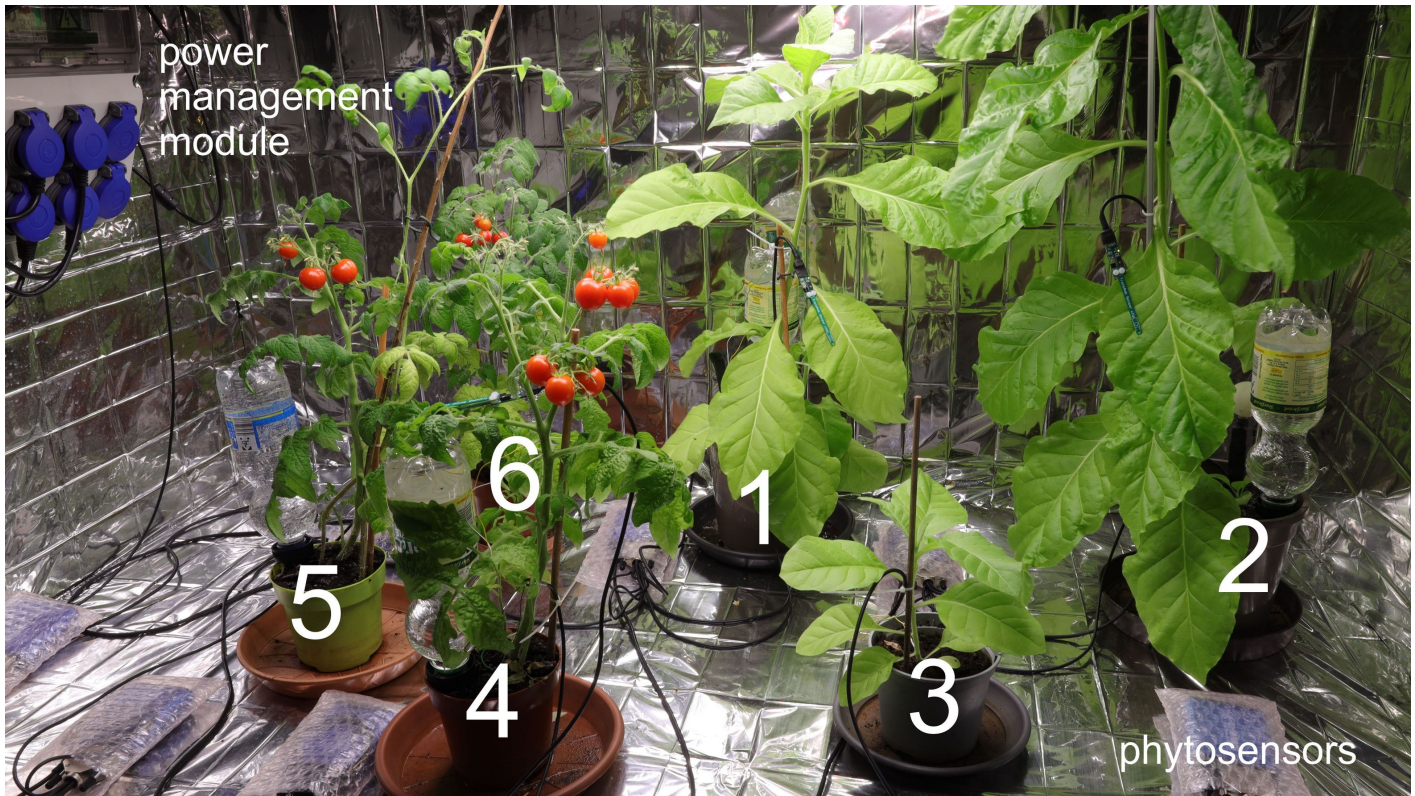


Figure 1. Measurement chamber with 3 tobacco and 3 tomato plants. Shown are phyto-sensors and the power management module for autonomous ON/OFF of light, aeration and preparing O_3 -air mix with the required O_3 concentration.



Figure 2. Placement of EIS electrodes with lower and upper positions.



Figure 3. Placement of the transpiration sensor.

5. To reduce the level of produced O_3 , the ozone generator is powered by 220V-PWM modulation with $<0.1\%$ of duty cycles.

The setup uses four different O_3 detectors/sensors: MQ131 Low (Winsen, 10–1000ppb, resolution: 1 ppb), ULPSM-O3 968-04 (SPEC, 0–20 ppm, resolution: 0.1ppm), DM509-O3 (0–5 ppm, resolution: 0.001 ppm), several measurements and calibrations have been done with POM (2B Technologies, 0–10 ppm, resolution: 1.5 ppb). Sensors are operated with 24 bit ADC in the data logger, and calibrated to a current level of atmospheric O_3 . Sec. II-A describes the used approach for generation and sensing of low O_3 concentrations in more detail.

Preparatory measurements demonstrated a dependency on the irrigation (soil, hydroponics, substrate + hydroponics), finally the best solution for such measurements represents a micro-

capillary irrigation with soil-based growth. A full spectra LED light is used as a light source. To prevent the plants from overheating, the measuring chamber is open on one side and has two continuously operating 200 mm fans. Since the temperature and humidity should be the same before and during ozone exposure, no intervention is made in the setup during daylight hours.

Outdoor setup. Outdoor setup has three tomato plants (*Solanum lycopersicum* 'Hellfruch') placed particularly in shadow to minimize heat stress, see Fig. 4. L- and R-plants have microcapillary irrigation (however they needed additional irrigation due to hot summer season), C-plant has the hydroponic+substrate solution for irrigation. This setup has the same placement of sensors as the indoor setup.



Figure 4. Outdoor setup with three tomato plants, arrows show lower and upper positions of EIS electrodes. Plants are placed in shadow however afternoon they are exposed to a direct sunlight, especially the L-plant.

Phytosensing in both setups is conducted by 6 (indoor) and 3 (outdoor) independent CYBRES phytosensing devices connected to PC via USB-to-USB isolators (to decrease noise and to avoid USB ground loops). In indoor setup, the power management module [22] is connected to one of phytosensors and enables remote/autonomous switching of light, aeration and preparation of O_3 -air mix.

Two physiological parameters are measured in all plants: tissues impedance in time-continuous mode with the fixed

excitation frequency (450Hz) in two locations with lower and upper positions of electrodes, see Fig. 2, and leaf transpiration, see Fig. 3. Additionally, soil moisture and temperature, air temperature and humidity, illumination, magnetic fields (by 3D magnetometer), air pressure and radio-frequency emission (450Mhz-2.5Ghz range) are recorded. Sampling rate is about 2 sps.

A. Generation and detection of low concentration of O_3

High concentration of ozone (>1 ppm) can be generated and detected by a number of different O_3 generators and sensors, it has an essential impact on plant physiology [9]. However, working with a low concentration of ozone (15-190 ppb over atmospheric O_3) represents some challenges for both generating and sensing parts. Due to PWM-modulation, O_3 from the generator should be first diluted in a large amount of air (in a preparatory chamber) and then pumped to the measurement chamber with plants. Low concentration of O_3 has inhomogeneous distribution of O_3 -air mix, it needs specific strategies for control a proper concentration of ozone. Different polymers are susceptible to oxidation by ozone [23], this creates additional local inequalities of O_3 distribution. Discovered issues on the sensing part are related to calibration of different O_3 sensors for low-scale measurements, inertially of sensor reaction on O_3 exposure and dependency to a measurement position due to inhomogeneous distribution of O_3 .

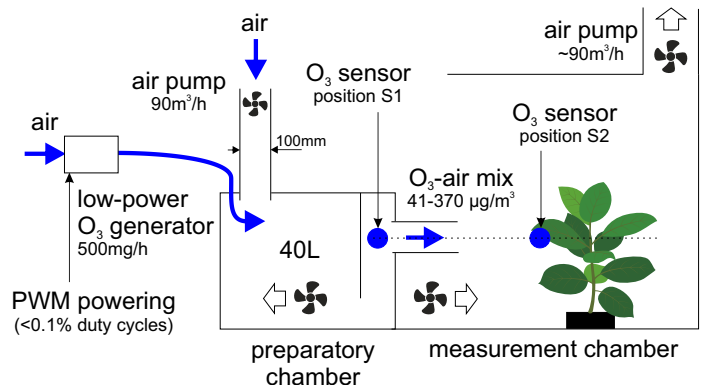


Figure 5. Scheme of experimental setup for generation and detection of low O_3 concentrations.

The used scheme of O_3 generation and distribution is shown in Fig. 5. Outputs of the air pump and O_3 generator are fed to a 40L preparatory chamber. O_3 generator is powered by 220V-PWM modulation with $<0.1\%$ of duty cycles (periodical on-off, e.g. on-time 2 sec., off-time 240 sec. – 2/240). The O_3 -air mix from the preparatory chamber enters to the measurement chamber with plants. Air fans distribute the O_3 -air mix and remove it from the laboratory to avoid accumulation of O_3 . ON/OFF switching of all elements is conducted remotely or autonomously by the power management module, connected to one of phytosensor devices; temperature and humidity are constant during experimental attempts, see supplementary Fig. 20.

Calibration of electrochemical O_3 sensors is performed based on their conversion diagrams to the level of atmospheric O_3 , see Fig. 11(a), considering humidity and temperature, and

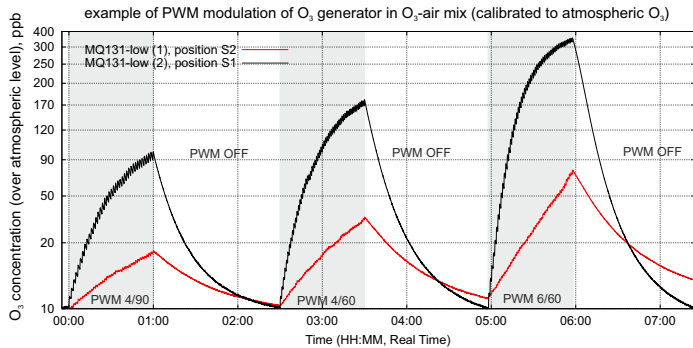


Figure 6. Examples of O_3 measurements and PWM modulation of O_3 -air mix in sensor positions S1 and S2 simultaneously by two equal O_3 sensors.

decomposition of O_3 to O_2 in laboratory [24]. Additionally, the calibration from conversion diagrams was compared to a factory-calibration of DM509- O_3 and POM meters. Based on these tests ULPSM- O_3 sensor was removed from measurements and POM was used only for initial calibrations of the PWM-based control, see Table I. Both MQ131 and DM509 connected to external 24 bit data logger provide a high resolution measurements in a low range of O_3 scale, however have different reaction time. O_3 generator produces ozone nonlinearly at short PWM impulses, see the coefficient $k_1=1.4-0.77$ in Table I, with longer PWM durations it generates disproportionately more O_3 .

Table I
 O_3 CONCENTRATIONS WITH DIFFERENT PWM SETTINGS OF O_3 GENERATOR (500 MG/H) AND CONSTANT AIR FLOW ($90 \text{ m}^3/\text{H}$), CONVERSION $\mu\text{G}/\text{M}^3$ TO PPB AT $T=27\text{C}$., DUE TO PWM-MODULATION THE MEASURED VALUES ARE ROUNDED TO INTEGERS.

PWM, sec/sec	expected $O_3, \mu\text{g}/\text{m}^3$	expected ppb	measured S1, O_3, ppb	$k_1, \text{exp./meas. S1}$	measured S2, O_3, ppb	$k_2, \text{meas. S1/S2}$
4/90	246.9	126.7	90-110	1.4-1.15	15-20	6-5.5
4/60	370.3	188.9	160-180	1.18-1.05	25-30	6.4-6
6/60	555.5	284.4	320-370	0.89-0.77	50-70	6.4-5.3
12/60	1111.1	570.1	-	-	>200	-

Since the measurement chamber is not closed in long-term measurements, O_3 concentration in it is lower than the set value in the preparatory chamber. We use two strategies for preparation of O_3 -air mix – by controlling O_3 in the preparatory or in measurement chambers (sensor positions S1 or S2). The first case guarantees that the eO_3 level does not overstep the set value, however ozone concentrations in the sensor position S2 are 6.4-5.3 times lower than in S1, see the coefficient k_2 in Table I and Fig. 6. In the second case we use the pumping strategy with excessive O_3 in S1 position during the fixed time and measure the actual ozone concentration in the position S2. Both strategies have impact on the O_3 dynamics. In experiments we used the excessive strategy with measurements by two equal O_3 sensors on the plant level (the position S2).

Finally, the range of 10-200 ppb O_3 is divided into two main

subranges, with max. 15-20 ppb and max. 50-70 ppb, in which most measurements were performed (O_3 exposure twice per day during 11:00-12:00 and 17:00-18:00). Note that the peak of O_3 exposure is only reached in a short period of time, see Figs. 6, 12(a). The ambient level of O_3 and the third range >200 ppb are used as control cases I and II to estimate the probability of false-negative and false-positive responses of biosensors.

B. Principles of EIS analysis in indoor setup

Example of EIS data taken from the tobacco 1 (T1) plant during 72 hours is shown in Fig. 7(a). Electrochemical dynamics is characterized by circadian rhythms indicating periodical movement of fluids in plant stem. An increase in electrochemical impedance means a decrease in the amount of ionic fluids in tissues (and vice versa). During the day we observe a slow decrease in fluid content through transpiration, while at night the roots supply the plant tissue with water (ionic aqueous solutions with dissolved minerals) and the fluid content increases. This is the simplest hydrodynamic model that explains the observed EIS dynamics, see [16] for more details.

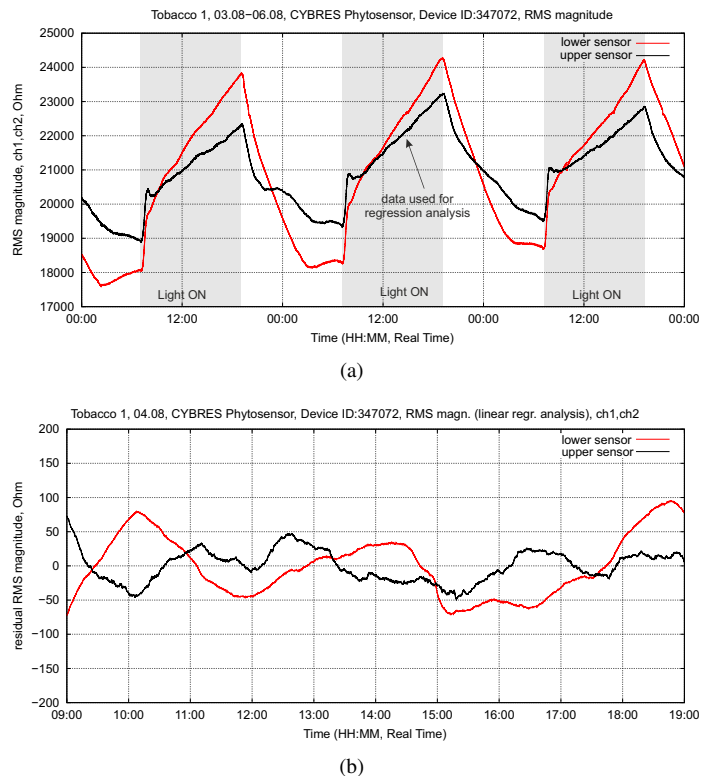


Figure 7. Example of EIS dynamics of upper and lower sensors: (a) Original EIS dynamics during 72 hours of the tobacco plant 1; (b) The regression analysis of daily time during 10 hours.

Day and night periods have a low noise dynamics (as long as the plants are not disturbed by additional stress), which can be processed by regression analysis. Fig. 7(b) shows an example of such an analysis for the interval 9.00–19.00 of a day period. We see that the 6000 Ohm variation is reduced to about 50 Ohm variation where all disturbances (e.g. applied O_3 stress) of the dynamics become detectable.

Such an analysis imposes several requirements: 1) the increase of ozone in the O_3 -air mix should occur in a short time

to achieve a significant change of electrochemical impedances; 2) the background period (without O_3 stress) should be long enough to provide good regression dynamics (periods without and with O_3 stress are typically in a 3:1 ratio); 3) plants should not be distorted by any other impacting factors such as temperature, humidity of irrigation, as they all affect the hydrodynamic system.

Fig. 8(a) shows the same plant with applied O_3 in the range of 15 ppb. Note that: 1) in most cases we only observe a change in electrochemical impedances in the upper sensor (increasing fluid content in the upper part of the stem associated with closing stomata); 2) the delay of biological response to applied O_3 is about 10–20 min.

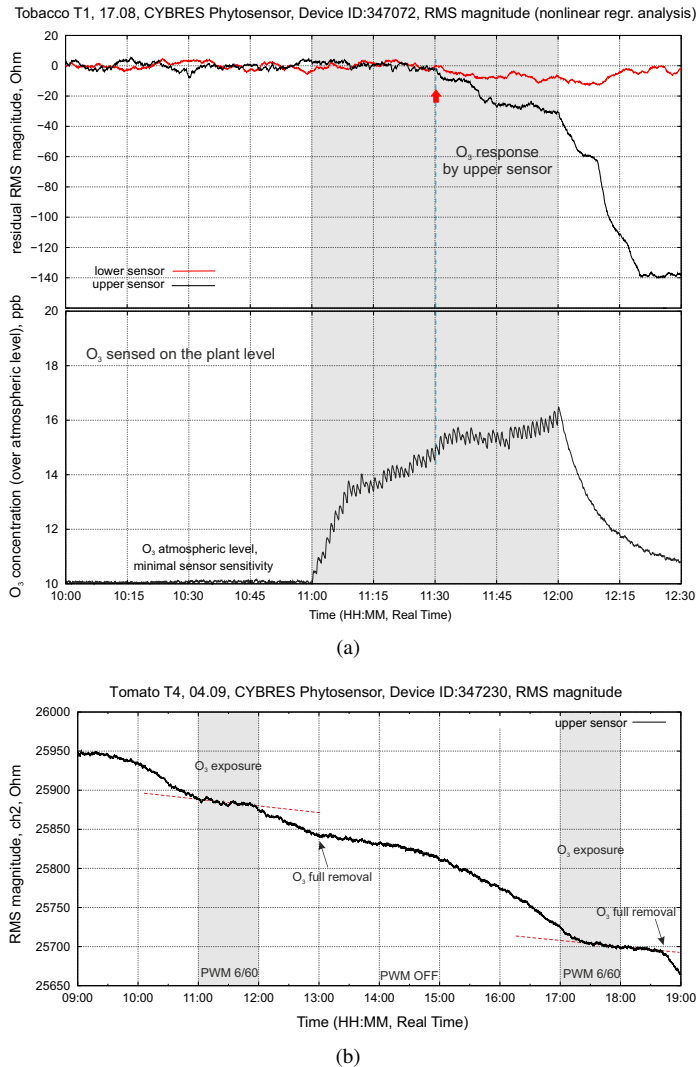


Figure 8. **(a)** Example of physiological response in the upper and lower positions of EIS sensors when exposed to low concentrations of O_3 ; **(b)** The type II EIS dynamics of tomato plants.

Examples of linear and nonlinear regression are shown in Fig. 9, their more detailed comparison with different regions of approximation and interpolation is shown in supplementary Fig. 19, and explained in [25]. It is important to note that the change in EIS trends should be within the exposure range (i.e., there must be a clear correlation between O_3 exposure and a change in EIS trend). The regression analysis allows calculating different

statistical or numerical parameters, see more in [26], [27], which enable accurate characterization of imposed stress.

Generally, we observe two types of EIS dynamics with increasing daily EIS trend as shown in Fig. 7(a), further the type I, and decreasing daily EIS trend as shown in Fig. 8(b), further the type II. The type I dynamics can be explained by decreasing fluid content due to transpiration, O_3 exposure reduces stomatal aperture and leads to decreasing EIS trend (higher fluid content in the stem) during exposure up to a full removal of O_3 from the lab. The regression analysis provides primarily a downward response for the type I.

The type II dynamics is demonstrated mostly in stress conditions, for instance, the outdoor setup shows the type II dynamics in 90.6% of all cases. During O_3 exposure, the EIS trend increases, the regression analysis demonstrates both upward and downward responses, see Fig. 12(b). Considering different O_3 -protective reactions [28], [29], here not only stomatal mechanisms are involved, but more complex hormonal regulation preventing toxic effects beyond the hydrodynamic system. Both types of EIS dynamics uses the same analysis, however their hypotheses should be tested during measurements.

The interference between irrigation and O_3 exposure is shown in Fig. 9 for tobacco and tomato plants. It initially distorts the hydrodynamic system near the roots and spreads along the stem to the upper parts. The disturbances last about 120–150 minutes. Taking into account the necessary background measurements, irrigation should be carried out at least 4–5 hours before O_3 exposure.

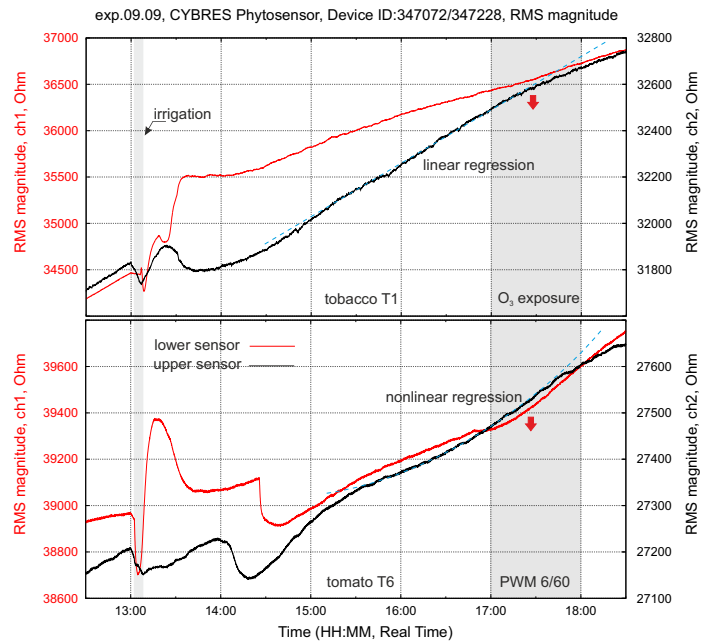


Figure 9. Interference between irrigation and O_3 exposure for tobacco and tomato plants. Both graphs exemplify also the linear and nonlinear regression used in the data analysis for the indoor setup.

C. Principles of EIS analysis in outdoor setup

There are two specific aspects of EIS dynamics that only occur outdoors: distortions produced by wind and rain, and artefacts produced by exposure to direct sunlight. If the distortion

areas still reflect the hydrodynamics of fluid transportation, the regions with artefacts cannot be used for analysis.

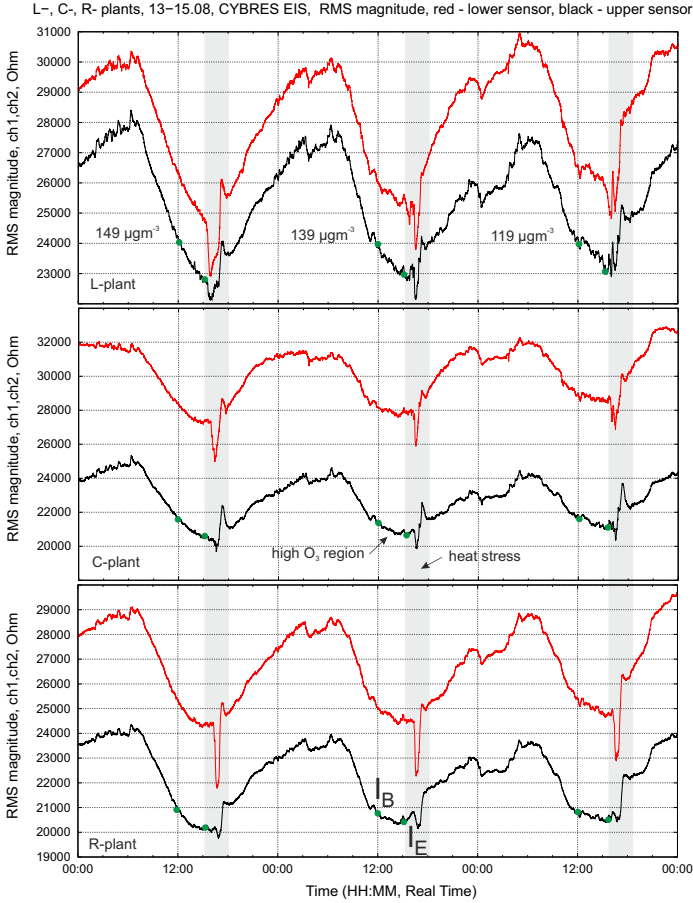


Figure 10. EIS dynamics from three tomato plants in outdoor setup during 72 hours, compare to Fig. 7 in indoor setup, shadow regions represent heat stress in afternoon time. Green points – the values I_B and I_E , see expression (6), mark the region with the highest daily O_3 concentration.

Fig. 10 shows the EIS dynamics of three tomato plants outdoors over 72 hours. Shadow areas show the heat stress (as well as UV/IR radiation) in the afternoon. Corresponding peaks are largely present in both sensors of L-plant (this plant and both sensors are mostly in sunlight in the afternoon), R-plant has only short peaks in the lower sensor (which is partially in sunlight). Obviously, such peaks do not reflect the movement of fluids, but other phenomena related to heat and UV/IR radiation that affect plant physiology and physical chemistry of EIS sensing [20].

Another clearly visible effect is related to circadian rhythms – the maximum impedance in indoor plants in Fig. 7(a) correlates with the end of lighting period (evening), while the maximum in outdoor plants is shifted to the morning (the type II of EIS dynamics). Taking into account that an increase in ozone leads to change of impedances in the upper sensor, we expect that EIS dynamics between 12.00 and 16.00 – the points I_B and I_E in Fig. 10 (beside artefact areas) on high-ozone days will have different contribution to 24-hours circadian rhythm compared to the same dynamics of low-ozone days.

Since the used O_3 sensors are not intended for long-term outdoor measurements, we used data from two local air mon-

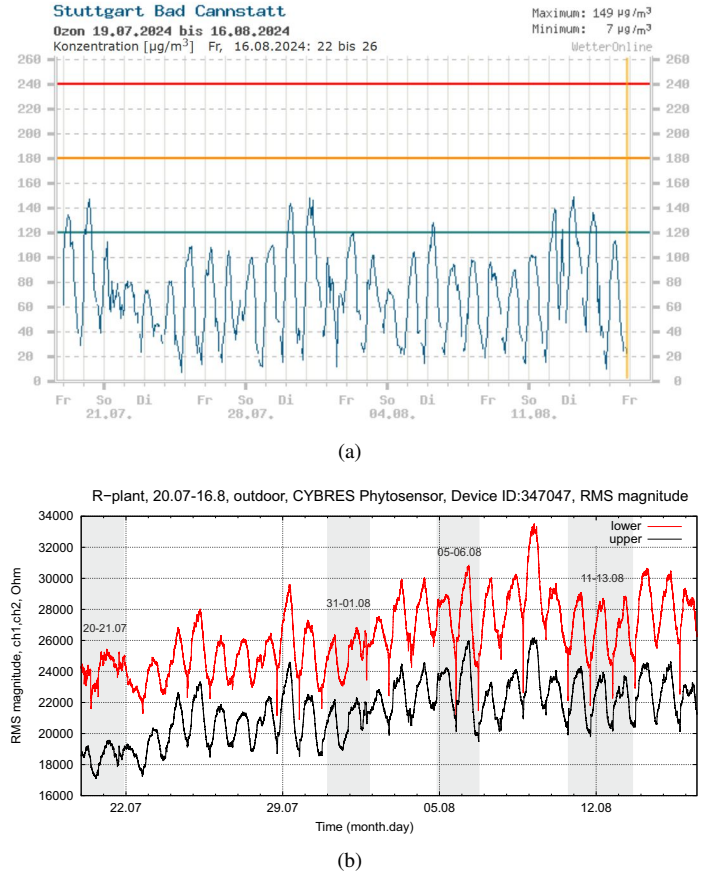


Figure 11. (a) Concentration of atmospheric O_3 during 27 days, data from the State Agency for the Environment Baden-Württemberg (Landesanstalt für Umwelt Baden-Württemberg), image from www.wetteronline.de/ozonwerte/stuttgart. (b) EIS dynamics the R-Plant, the high-ozone days are marked by grey areas

itoring stations in outdoor measurements. Fig. 11(a) shows a concentration of atmospheric O_3 during experiments from such a station, daily values range between 80 and 100 μgm^{-3} that corresponds to 40.8 – 50.9 ppb (1 ppb = 1.96 μgm^{-3} at 25C), the largest value is 149 μgm^{-3} or 75.9 ppb. Fig. 11(b) shows EIS dynamics of R-plant in the same period, the high-ozone days are marked by grey areas. The ideas of analysis can be based on comparison of $\Delta I = I_B - I_E$ values on high- O_3 and low- O_3 days. Ozone stress changes the inclination of $I_B - I_E$ region, we expect that numerical value of ΔI will reflect this impact. Since different circadian cycles are shifted to each other, it needs to analyse pairwise ΔI_{highO_3} and ΔI_{lowO_3} from similar regions of long-term EIS dynamics. Next section demonstrates this analysis.

III. RESULTS

Indoor setup. In general, the circadian EIS dynamics is specific for each plant species and environmental conditions, compare Figs. 10 and 22 for outdoor and indoor tomatoes and Fig. 7 for tobacco. However, all plants of the same species and in the same conditions demonstrated a homogeneous reaction on O_3 exposure, see supplementary Fig. 23. Comparing a reaction on different concentrations of O_3 (about 190 ppb, 60 ppb, 20 ppb), we see a small shift of inflection points (about 7-10 min

Table II
 PROBABILITY OF A TYPE I REACTION UPON EXPOSURE TO O₃, THE INDOOR SETUP WITH T1-T6 PLANTS, N – THE NUMBER OF PLANT-SENSOR ATTEMPTS, S_L – LOWER EIS SENSOR, S_U – UPPER EIS SENSOR. CASES 11:00-12:00 AND 17:00-18:00 ACCUMULATE REACTIONS OF ALL PLANTS IN ALL DAYS AT THESE ATTEMPTS.

PWM	O ₃ , ppb	N	plant T1		plant T2		plant T3		plant T4		plant T5		plant T6		11:00-12:00		17:00-18:00		
			S _L	S _U	S _L	S _U	S _L	S _U	S _L	S _U	S _L	S _U	S _L	S _U	S _L	S _U	S _L	S _U	
1	control	—	180	0.20	0.13	0.20	0.13	0.27	0.13	0.07	0.07	0.13	0.20	0.13	0.13	0.19	0.14	0.15	0.13
2	4/90	15-20	204	0.71	0.65	0.47	0.76	0.35	0.53	0.53	0.47	0.53	0.76	0.53	0.88	0.40	0.73	0.63	0.63
3	6/60	50-70	252	0.43	0.76	0.33	0.86	0.52	0.62	0.33	0.57	0.38	0.86	0.52	0.90	0.32	0.80	0.52	0.73
4	12/60	>200	132	0.27	0.64	0.73	0.91	0.91	0.91	0.55	0.73	0.18	0.91	0.36	0.82	0.53	0.93	0.43	0.80

in each case) and also proportional inclination of EIS curves for both type I and type II responses, see Fig. 12. This demonstrates a possibility of qualitative but also quantitative measurements after calibration. We also note more evident reactions by tobacco with clear inflection points even for small concentrations of O₃ (<20ppb).

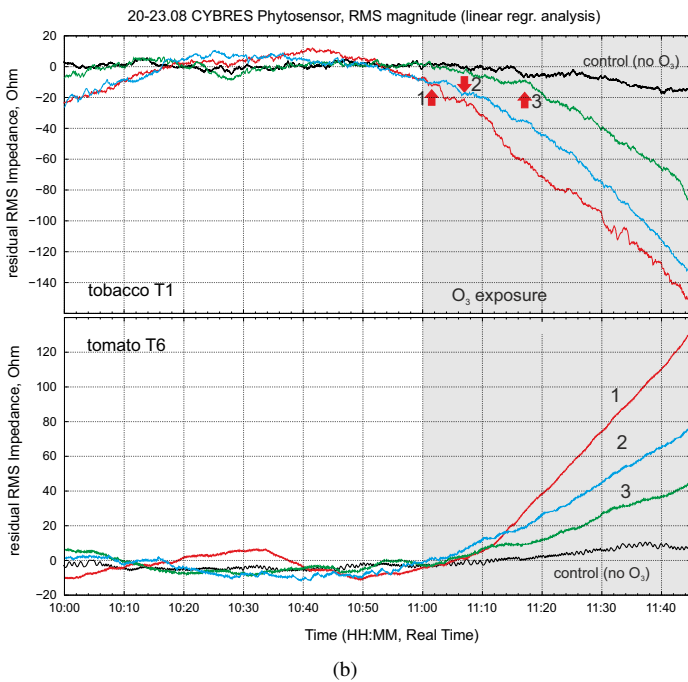
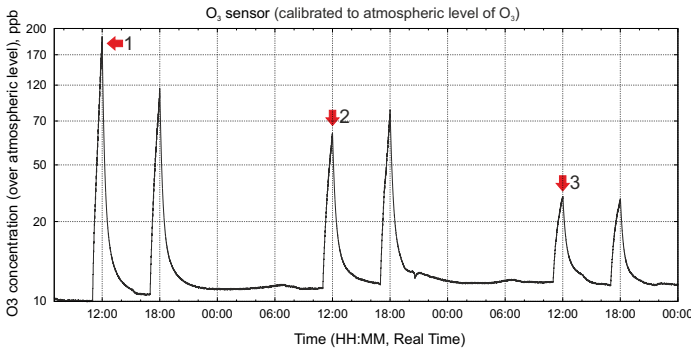


Figure 12. (a) Test with different concentrations of O₃; (b) Reactions of tobacco and tomato plants (linear regression analysis): shift of inflection points and proportional inclination of EIS curves for both type I and type II responses.

Analysis is conducted automatically, for this the EIS dynam-

ics is divided into 120 min of background region B and 60 min of experimental region (O₃ exposure) E . Since the physiological reaction is delayed after the PWM is ON, E is shifted by 30 min after the exposure starts. The original data $data(x)$ in the background region B from EIS devices are approximated by the nonlinear function $fit_N(x)$ of 5th order, using the Levenberg-Marquardt algorithm [30], where we consider the residual curve

$$R(x) = fit_{L,N}(x) - data(x). \quad (1)$$

Finally, standard deviations σ for $R(x)$ curve are calculated; σ_B characterizes the background, σ_E characterizes the experimental regions. The ratio

$$\Psi = k \frac{\sigma_E}{\sigma_B} \quad (2)$$

represents the final result: the more intense is the perturbations of the region E in relation to B , the higher is the value of Ψ . The coefficient k reflects the downward or upward trend, $k = -1$ if EIS dynamics goes down in the E phase (less than zero) and $k = 1$ – otherwise. Since the EIS sensor has lower and upper channels, we calculate Ψ_L and Ψ_U for each experimental case. If $\Psi_U > 0$ is received, the analysis is repeated by setting the E region to the start of O₃ exposure, the lower from these results is collected in the Table II. This step allows avoiding artefacts of regression analysis caused by wrong recognition of physiological response. Additionally, the values $R_E(x)$ (value of $R(x)$ at the end of experimental region E) are also recorded.

First, we test the hypotheses about type I and type II dynamics by analysing the $\Psi < 0$ conditions. All O₃ exposures are coded by

$$1 : \Psi < 0, \quad (3)$$

$$0 : \Psi > 0. \quad (4)$$

All 0 and 1 are collected per plant, sensor and experimental series, and normalized to the [0..1] range. They can be considered as the probability of a type I reaction upon exposure to O₃. Table II shows these results. We see that the type I dynamics represents >50% for the upper sensor, plants T2, T5 and T6 have >75% of type I dynamics, thus the condition (3) will be counted as the main sensor response.

The control series accumulate measurements conducted before experimental series and between them. Since approximation-interpolation approach will always deliver a small deviation, for the control cases we additionally require

$$|R_R(x)| > 10, \quad (5)$$

to avoid a wrong detection of low amplitude changes. In control measurements we observe the probability 0.07-0.27 (0.15±0.06)

of false-positive response. The false-negative detections for the type I dynamics include both the type II hypothesis and non-responsive measurements – we observe an increase in type II reactions in the last series with >200 ppb. The probability of false-negative detection can be roughly estimated from the >200 ppb case (upper sensor forenoon and afternoon) – between 0.07 and 0.20. However, we emphasize that this is a specific form of false-negative results and can be improved by detecting biological reactions that include both type I and type II dynamics.

Both false-positive and false-negative reactions are explained by internal physiological dynamics, reactions to other stress factors, as well as by the regression analysis that requires a flat EIS dynamics in the B region. Young plants, such as the T3 plant, have a lower level of reaction, their usage in phytosensing should be avoided. It needs also to pay attention on the high-performance biosensors, such as the tomato T6 plant, which has 0.88, 0.9 and 0.82 reactions on O_3 exposures.

We additionally analysed a combination of data from several plants, which improves a reliable identification of excessive O_3 . Such a combined biosensor represents the main practical interest. Three phytosensors operating in parallel (T2, T5, T6 with $>75\%$ of type I dynamics), provide 0.82 and 0.92 reaction based on majority decision, see Fig. 13.

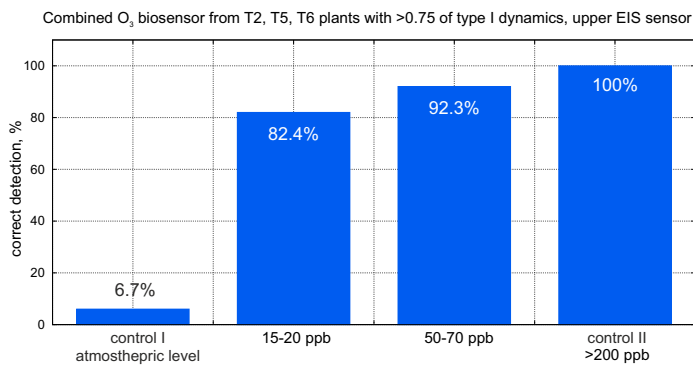


Figure 13. Combined sensor based on the type I dynamics – combination of data (majority decision) from three phytosensors operating in parallel (T2, T5, T6 with $>75\%$ of type I dynamics).

Another interesting result is related to detection of excessive O_3 by upper and lower EIS sensors, see Fig. 14. Upper sensors provide better results for both 11:00-12:00 and 17:00-18:00 attempts. They also reflect the quantitative aspect shown in Fig. 12 – an increase in O_3 leads to a stronger physiological response. We see that the position of electrodes plays an important role in the biosensor and reflects different physiological processes in the root and leaf area.

Outdoor setup. During 51 days of measurements (19.07-07.09) the local air monitoring station counted 15 days when the O_3 concentration overstepped $120 \mu\text{gm}^{-3}$ (about $130 \mu\text{gm}^{-3}$ in average). Due to possible O_3 variations between the pollution station and measurement location (about 3 km distance), we used data from two such stations (Stuttgart Bad-Cannstatt and Stuttgart Arnulf-Klett-Platz). We also selected 15 days with low O_3 concentration (about $80 \mu\text{gm}^{-3}$ in average). Minimal difference between low-ozone and high-ozone days is about $40\text{--}50 \mu\text{gm}^{-3}$, which is comparable to the case 2 in indoor setup with 15-20 ppb range. These two data sets represent control and experimental cases.

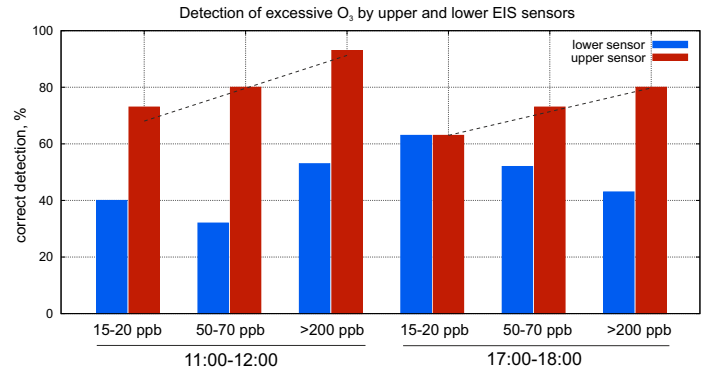


Figure 14. Detection of excessive O_3 by upper and lower EIS sensors.

For analysis we tested first the already discussed approach with the type II dynamics

$$\Delta I = I_B - I_E > 0, \quad (6)$$

where I_B , I_E impedances of two regions of circadian rhythm at the begin and end of measurements (tested are three settings for $I_B - I_E$ as 12:00-16:00, 12:00-17:00 and 12:00-18:00). From 180 measurements (30 high/low O_3 days x 3 plants x 2 sensor locations), only 9.4% are type I EIS dynamics, and 90.6% – type II dynamics. I_B , I_E are calculated based on the mean of 10 EIS points. ΔI from all three plant in the outdoor setup (upper position of EIS sensors, 12:00-16:00 region of measurements) are shown in Fig. 15.

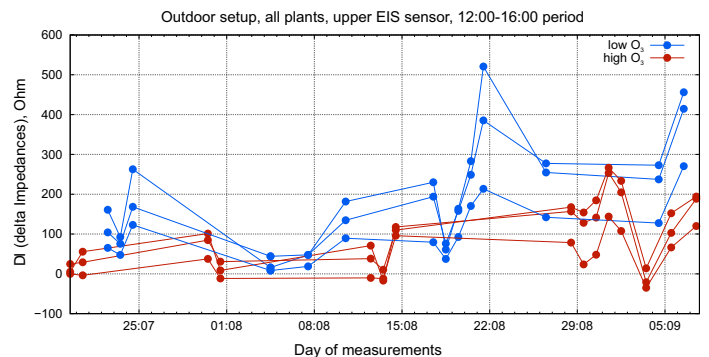


Figure 15. Values of ΔI from all three plant in outdoor setup, upper position of EIS sensors, 12:00-16:00 region of measurements, black and red points are low/high O_3 days, used in measurements

Since the dynamics of ΔI is not normalized (it includes trend from different stressors), we apply the analysis of means for a combination of EIS sensors from different plants, Fig. 16 demonstrates a separability of high/low O_3 sets for the selection 8 of 12 EIS data (3 plants x 2 EIS sensors x 2 high/low O_3 sets). Here we apply the same approach that is used in the indoor setup – a combination of different sensors and different plants can improve the overall quality of sensing. Separability is one of the most important practical results because it enables the application of different pattern recognition approaches used in machine learning.

Finally, a comparison of means for all sensors and plants is shown in Fig. 17. We can see that the best ratio for high/low O_3 recognition – high to low ratio 2.32 or low to high ratio 0.43 – it obtained for the R-plant (the plant in shadow with

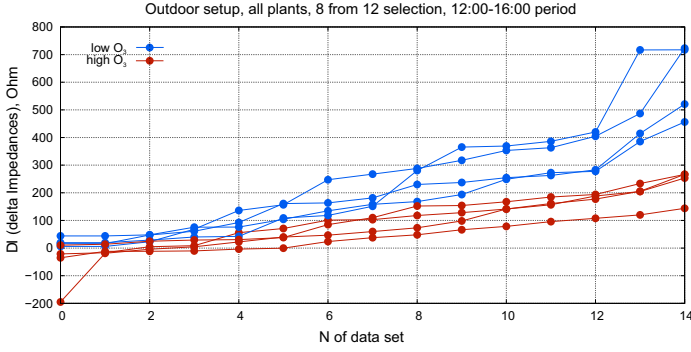


Figure 16. Separability of high/low O_3 sets for the selection 8 of 12 EIS data – combination of measurements from different sensors and plants (measurements points are sorted by increasing values).

minimal additional stress) and upper EIS sensor. Note that selecting I_B-I_E as 12:00-17:00 or 12:00-18:00 that include heat and IR/UV impacts, see supplementary Fig. 24, the dynamics of ΔI receives large random components and the expression (6) is no longer consistent. This demonstrates the importance of protecting measurement plants from direct sun radiation in outdoor conditions. Concluding the analysis of outdoor setup, we observe that a high O_3 concentration decreases the amplitude of EIS dynamics, which is also consistent with the type II dynamics of tomato plants in the indoor setup, see Fig. 8(b).

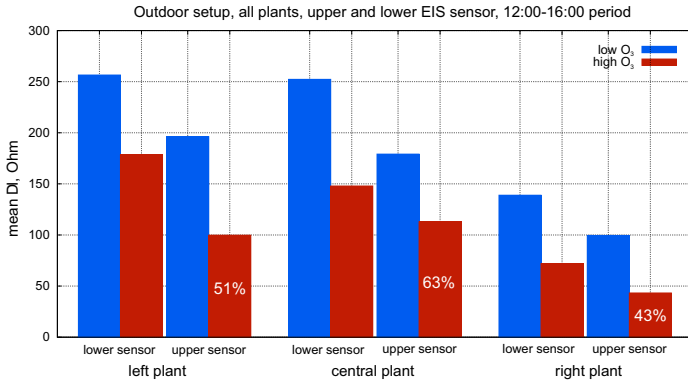


Figure 17. Comparison of means for all sensors and plants for 12:00-16:00 measurement region, numbers show the relation between high/low O_3 recognition by the same sensor, for instance, the low to high ratio 0.43 (or high to low ratio 2.33) is obtained for the R-plant and upper EIS sensor.

IV. DISCUSSIONS

One of the main methodological issues concerns type I vs. type II dynamics. In the selected analytical approach, we first test the hypothesis and then analyze the exposed EIS dynamics of O_3 based on this test. This leads to incorrect inclusion of 9% – 25% (outdoor–indoor) of correct results in false-negative cases. The switching between type I and type II dynamics has physiological reasons that need to be investigated in more detail. Applying other types of analysis, e.g. based on neural networks, can potentially improve the level of correct detections.

Another point of discussion in the indoor setup is related to the two-step dilution scheme of O_3 to 41-370 $\mu\text{g}/\text{m}^3$ from 500 mg/h generator. The first step is isolated from the setup in the

preparatory chamber, so that we can guarantee that high O_3 concentrations will not affect the plants even in a short time. However, the second step between sensor positions S1 and S2 is conducted in the measurement chamber with plants. Potentially, local O_3 inhomogeneity can reach some plants for a short time (in term of a few seconds considering two continuously operating 200m fans). Since EIS dynamics demonstrates a response in 10-20 minutes after the onset of exposure, we argue that such potential short term O_3 inhomogeneities will not essentially affect the EIS dynamics.

The O_3 concentration has a typical pumping behaviour, from the atmospheric level up to the maximal value as shown in Fig. 6. Moreover, due to the O_3 to O_2 decomposition, the laboratory level of O_3 (e.g. reached over night) is lower than the environmental concentration. The lowest range calibration of all used sensors and meters has a specific absolute inaccuracy at beginning of the scale despite very precise relative measurements, moreover both O_3 -sensors and O_3 -generator have a nonlinearity at lower O_3 values. Considering these points, we can speak only about ranges of O_3 exposure over the current atmospheric level. This situation reflects the outdoor exposure, where O_3 level has a sinusoidal daily dynamics and typically we refer to a maximal O_3 level reached on that day.

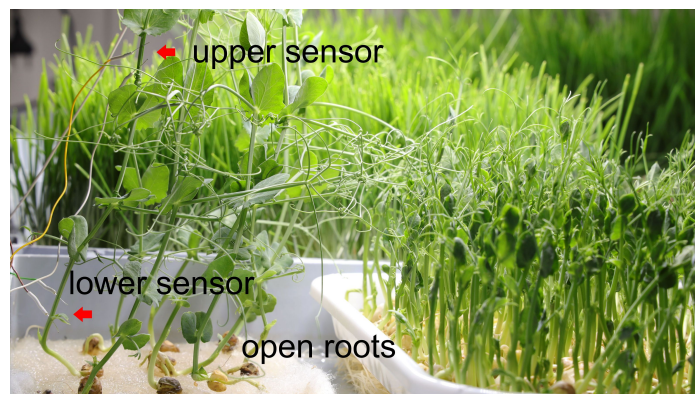
One of most serious issues in the outdoor setup is related to overlapping of different stress factors (wind, rain, heat, UV/IR radiation) as shown in Fig. 10. Some of these factors affect the whole physiology, other only EIS sensing processes on the level of physical chemistry (in particular, the UV/IR radiation [20]). Since the outdoor setup shown in Fig. 4 has a well-defined exposure time to direct sunlight, we remove these intervals for each plant individually. More generally, if plants are used as biosensors for environmental O_3 (or any other pollutant), they have to be protected from additional stress factors (or at least from a direct sunlight). This is also related to environmental sensors, for instance temperature/humidity sensors should not be exposed to a direct sunlight.

A separate point of discussion is the selectivity of biosensors to a specific environmental pollutant. In conducted experiments, we also noted a physiological response to PM (particulate matter), moreover, O_3 is correlated with nitrogen oxides (NOx) [31]. If we consider nonspecific physiological responses of plants at the hydrodynamic level, we can refer EIS-based biosensors to sensors that detect a biological response to complex environmental pollution from various sources.

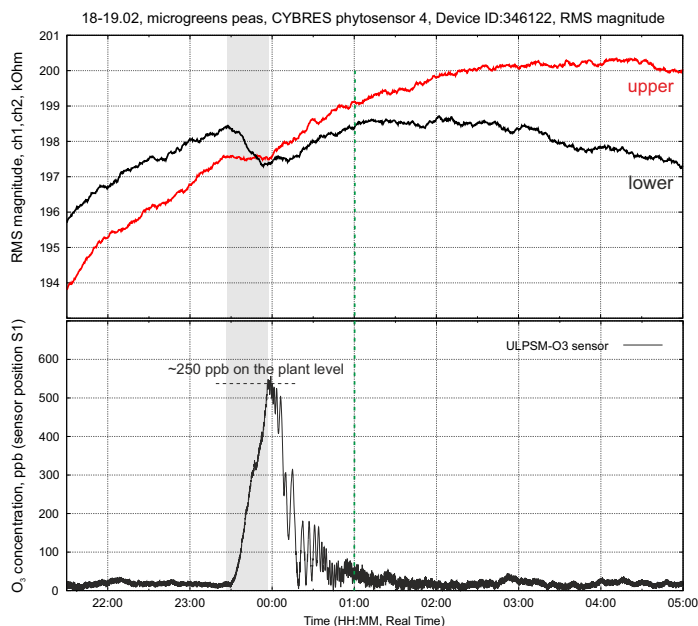
Interesting observation is made within preliminary tests with microgreens in vertical farm, see Fig. 18(a). As is typical for wheat and peas, their cultivation is conducted without soil/substrate with open roots and frequent periodical irrigation [16]. Exposure to O_3 demonstrated a higher response of the lower sensor, indicating a reaction of roots on ozone, see Fig. 18(b). Given the limited information on the mechanism of action of ozone on roots and the ongoing discussion [32], such setups can be used to systematically investigate the impacts of environmental pollutants on new agricultural systems.

V. CONCLUSION

In this work we demonstrated a biological detection of a low concentration of O_3 by measuring electrochemical impedances of tissues in tobacco and tomato plants. Two setups have been



(a)



(b)

Figure 18. (a) Example of pea production in vertical farm without soil/substrate with open roots; (b) the response of EIS dynamics on O_3 exposure.

created focused on isolating only O_3 stress and performing a sufficient number of iterative experiments (indoor), and estimating complex influence from different environmental stressors (outdoor). The lower range of generated ozone in the O_3 -air mix is about $30 \mu\text{gm}^{-3}$ over the atmospheric level, where all plants demonstrated a stable response. Measurement results indicate a well detectable reaction of hydrodynamic system to changes of O_3 concentration in the upper part of stem (measured by upper EIS sensor) with a delay of 10-20 minutes between the onset of exposure and biological response. The difference between low- and high-ozone days is also detectable outdoors with $40\text{-}50 \mu\text{gm}^{-3}$ difference between low/high O_3 cases. By combining data from different plants in both setups, the detection rate was increased to 92% and low/high O_3 cases were clearly separated for pattern recognition algorithms and machine learning techniques. There are several methodological issues related to recognition of physiological reactions, O_3 generation and protection of plants in outdoor setup – they can be improved in further attempts. EIS sensors prove to be

extremely reliable, especially in harsh outdoor conditions. They also seem to be well suited for environmental monitoring and biosensing in addition to applications in precision agriculture and vertical farming.

VI. ACKNOWLEDGEMENT

This research was funded by European Union under Horizon 2020 research and innovation program, Grant Agreement No. 101017899, ‘WATCHPLANT: Smart Biohybrid Phyto-Organisms for Environmental In Situ Monitoring’. Author would like to thank Antonio Diaz Espejo (Institute for Natural Resources and Agrobiology, IRNAS-CSIC, Sevilla, Spain) for providing tobacco seeds and fruitful discussions about plant physiology as well as all members of CYBRES team and WATCHPLANT consortium for technical discussions on phytosensing and setup development.

VII. CONFLICTS OF INTEREST

The author declares that the research was conducted in the absence of any commercial or financial relationships that could be construed as a potential conflict of interest. The funders had no role in the design of the study; in the collection, analyses, or interpretation of data; in the writing of the manuscript; or in the decision to publish the results.

REFERENCES

- [1] L. Jimenez-Montenegro, M. Lopez-Fernandez, E. Gimenez, [Worldwide research on the ozone influence in plants](https://doi.org/10.3390/agronomy11081504), *Agronomy* 11 (8) (2021). doi: 10.3390/agronomy11081504. URL <https://www.mdpi.com/2073-4395/11/8/1504>
- [2] S. Karmakar, A. Baul Das, C. Gurung, C. Ghosh, Effects of ozone on plant health and environment: A mini review, *Research Journal of Agricultural Sciences* 13 (2022) 612–619.
- [3] L. O. Morales, A. Shapiguzov, O. Safronov, J. Leppala, L. Vaahtera, D. Yarmolinsky, H. Kollist, M. Brosche, Ozone responses in Arabidopsis: beyond stomatal conductance, *Plant Physiology* 186 (1) (2021) 180–192. doi:10.1093/plphys/kiab097.
- [4] N. Dusart, M.-N. Vaultier, J.-C. Olry, C. Bure, J. Gerard, Y. Jolivet, D. Le Thiec, Altered stomatal dynamics of two euramerican poplar genotypes submitted to successive ozone exposure and water deficit, *Environmental Pollution* 252 (2019) 1687–1697. doi:https://doi.org/10.1016/j.envpol.2019.06.110.
- [5] M. M. Hasan, M. Rahman, M. Skalicky, N. M. Alabdallah, M. Waseem, M. Shah Jahan, G. J. Ahammed, X. Fang, M. Ibrahim, A. Abou El-Yazied, Ozone induced stomatal regulations, mapk and phytohormone signaling in plants, *International Journal of Molecular Sciences* 22 (2021) 1–14. doi:10.3390/ijms22126304.
- [6] Y. Hoshika, G. Katata, M. Deushi, M. Watanabe, T. Koike, Ozone-induced stomatal sluggishness changes carbon and water balance of temperate deciduous forests, *Scientific Reports* 5 (2015) 9871. doi:10.1038/srep09871.
- [7] L. García-Carmona, S. Bogdan, A. Diaz-Espejo, M. Dobilewski, H. Hamann, V. Hernandez-Santana, A. Kernbach, S. Kernbach, A. Quijano-López, N. Roxhed, B. Salamat, M. Wahby, Biohybrid systems for environmental intelligence on living plants: Watchplant project, in: *Proceedings of the Conference on Information Technology for Social Good, GoodIT '21, Association for Computing Machinery, New York, NY, USA, 2021*, pp. 210–215. doi:10.1145/3462203.3475885.
- [8] H. Hamann, S. Bogdan, A. Diaz-Espejo, L. Garcia Carmona, V. Hernandez-Santana, S. Kernbach, A. Kernbach, A. Quijano-Lopez, B. Salamat, M. Wahby, Watchplant: Networked bio-hybrid systems for pollution monitoring of urban areas, *ALIFE 2021: The 2021 Conference on Artificial Life*, 2021. doi:10.1162/isal_a_00377.
- [9] E. Buss, T. Aust, M. Wahby, T.-L. Rabbel, S. Kernbach, H. Hamann, Stimuli classification with electrical potential and impedance of living plants: Comparing discriminant analysis and deep learning methods, *Bioinspiration & biomimetics* 18 (02 2023). doi:10.1088/1748-3190/acbad2.

- [10] G. H. Kerr, D. W. Waugh, S. D. Steenrod, S. A. Strode, S. E. Strahan, Surface ozone-meteorology relationships: Spatial variations and the role of the jet stream, *Journal of Geophysical Research: Atmospheres* 125 (21) (2020) e2020JD032735. doi:<https://doi.org/10.1029/2020JD032735>.
- [11] K. A. Keerthi Lakshmi, T. Nishanth, M. K. Satheesh Kumar, K. T. Valsaraj, A comprehensive review of surface ozone variations in several indian hotspots, *Atmosphere* 15 (7) (2024). doi:[10.3390/atmos15070852](https://doi.org/10.3390/atmos15070852). URL <https://www.mdpi.com/2073-4433/15/7/852>
- [12] S. Kernbach, Electrochemical characterisation of ionic dynamics resulting from spin conversion of water isomers, *Journal of The Electrochemical Society* 169 (6) (2022) 067504. doi:[10.1149/1945-7111/ac6f8a](https://doi.org/10.1149/1945-7111/ac6f8a).
- [13] Y. Liu, D. Li, J. Qian, B. Di, G. Zhang, Z. Ren, Electrical impedance spectroscopy (eis) in plant roots research: a review, *Plant Methods* 17 (11) (2021). doi:[10.1186/s13007-021-00817-3](https://doi.org/10.1186/s13007-021-00817-3).
- [14] K. Jin, J. Shen, R. Ashton, R. White, I. Dodd, A. Phillips, M. Parry, R. Whalley, The effect of impedance to root growth on plant architecture in wheat, *Plant and Soil* 392 (07) (2015). doi:[10.1007/s11104-015-2462-0](https://doi.org/10.1007/s11104-015-2462-0).
- [15] M. Van Haeverbeke, B. De Baets, M. Stock, Plant impedance spectroscopy: a review of modeling approaches and applications, *Frontiers in Plant Science* 14 (2023). doi:[10.3389/fpls.2023.1187573](https://doi.org/10.3389/fpls.2023.1187573).
- [16] S. Kernbach, Biofeedback-based closed-loop phytoactuation in vertical farming and controlled-environment agriculture, *Biomimetics* 9 (10) (2024). doi:[10.3390/biomimetics9100640](https://doi.org/10.3390/biomimetics9100640).
- [17] S. C. Agathokleous E, Zhang K, Model-based estimation of the leaf area of ozone-indicator tobacco (*nicotiana tabacum* L.) plants under ambient ozone conditions, *MethodsX* (2023) 102214. doi:[10.1016/j.mex.2023.102214](https://doi.org/10.1016/j.mex.2023.102214).
- [18] H. E. Heggstad, Ozone as a tobacco toxicant, *Journal of the Air Pollution Control Association* 16 (12) (1966) 691–694. doi:[10.1080/00022470.1966.10468534](https://doi.org/10.1080/00022470.1966.10468534).
- [19] V. Calatayud, M.-J. Sanz-Sanchez, E. Calvo Rosello, J. Cerver, W. Ansel, A. Klumpp, Ozone biomonitoring with bel-w3 tobacco plants in the city of valencia (spain), *Water, Air, and Soil Pollution* 183 (2007) 283–291. doi:[10.1007/s11270-007-9376-2](https://doi.org/10.1007/s11270-007-9376-2).
- [20] A. Wang, G. H. Pollack, Effect of infrared radiation on interfacial water at hydrophilic surfaces, *Colloid and Interface Science Communications* 42 (2021) 100397. doi:[10.1016/j.colcom.2021.100397](https://doi.org/10.1016/j.colcom.2021.100397).
- [21] S. Kernbach, O. Kernbach, I. Kuksin, A. Kernbach, Y. Nepomnyashchiy, T. Dochow, A. Bobrov, The biosensor based on electrochemical dynamics of fermentation in yeast *Saccharomyces Cerevisiae*, *Environmental Research* 213 (2022) 113535. doi:[10.1016/j.envres.2022.113535](https://doi.org/10.1016/j.envres.2022.113535).
- [22] S. Kernbach, Application Note 28. Using phytosensor in precision agriculture, vertical farms, hydroponics and agricultural AI applications, CYBRES GmbH, 2024. URL http://cybertronica.de.com/download/CYBRES_Application_Note_28.pdf
- [23] A. Kefeli, S. Razumovskii, G. Zaikov, Interaction of polyethylene with ozone, *Polymer Science U.S.S.R.* 13 (4) (1971) 904–911. doi:[https://doi.org/10.1016/0032-3950\(71\)90288-7](https://doi.org/10.1016/0032-3950(71)90288-7). URL <https://www.sciencedirect.com/science/article/pii/0032395071902887>
- [24] T. Batakliiev, V. Georgiev, M. Anachkov, S. Rakovsky, G. Zaikov, Ozone decomposition, *Interdisciplinary toxicology* 7 (2014) 47–59. doi:[10.2478/intox-2014-0008](https://doi.org/10.2478/intox-2014-0008).
- [25] CYBRES, Differential Impedance Spectrometer for electrochemical and electrophysiological analysis of fluids and organic tissues. Handbook and User Manual, CYBRES GmbH, 2024. URL https://cybertronica.co/download/MU-EIS_Manual_en.pdf
- [26] S. Kernbach, Application Note 27. Using regression scan for electrochemical 'treatment-during-measurement' experiments, CYBRES GmbH, 2020. doi:[10.13140/RG.2.2.24161.93280](https://doi.org/10.13140/RG.2.2.24161.93280). URL http://cybertronica.de.com/download/CYBRES_Application_Note_27.pdf
- [27] S. Kernbach, Application Note 24. Analysis of electrochemical fluctuations for fast impedance spectroscopy, CYBRES GmbH, 2018. doi:[10.13140/RG.2.2.10504.23047](https://doi.org/10.13140/RG.2.2.10504.23047). URL http://cybertronica.de.com/download/CYBRES_Application_Note_24.pdf
- [28] I. Super, J. Vilà-Guerau de Arellano, M. C. Krol, Cumulative ozone effect on canopy stomatal resistance and the impact on boundary layer dynamics and co2 assimilation at the diurnal scale: A case study for grassland in the netherlands, *Journal of Geophysical Research: Biogeosciences* 120 (7) (2015) 1348–1365.
- [29] M. M. Hasan, M. A. Rahman, M. Skalicky, N. M. Alabdallah, M. Waseem, M. S. Jahan, G. J. Ahammed, M. M. El-Mogy, A. A. El-Yazied, M. F. M. Ibrahim, X.-W. Fang, Ozone induced stomatal regulations, mapk and phytohormone signaling in plants, *International Journal of Molecular Sciences* 22 (12) (2021). doi:[10.3390/ijms22126304](https://doi.org/10.3390/ijms22126304). URL <https://www.mdpi.com/1422-0067/22/12/6304>
- [30] J. Dennis, R. Schnabel, Numerical methods for unconstrained optimization and nonlinear equations, Prentice-Hall Series in Computational Mathematics, Englewood Cliffs, 1983. doi:[10.1137/1.9781611971200](https://doi.org/10.1137/1.9781611971200).
- [31] A. Souza, F. Aristone, U. Kumar, E. Kovac-Andric, M. Velickovic, P. Ikefuti, Analysis of the correlations between no, no2 and o3 concentrations in campo grande – ms, brazil, *European Chemical Bulletin* 6 (2017) 284. doi:[10.17628/ecb.2017.6.284-291](https://doi.org/10.17628/ecb.2017.6.284-291).
- [32] Z. Chen, H. Yu, H. Shang, J.-X. Cao, Effects of ozone stress on tree root: a review 29 (2016) 455–463.

APPENDIX

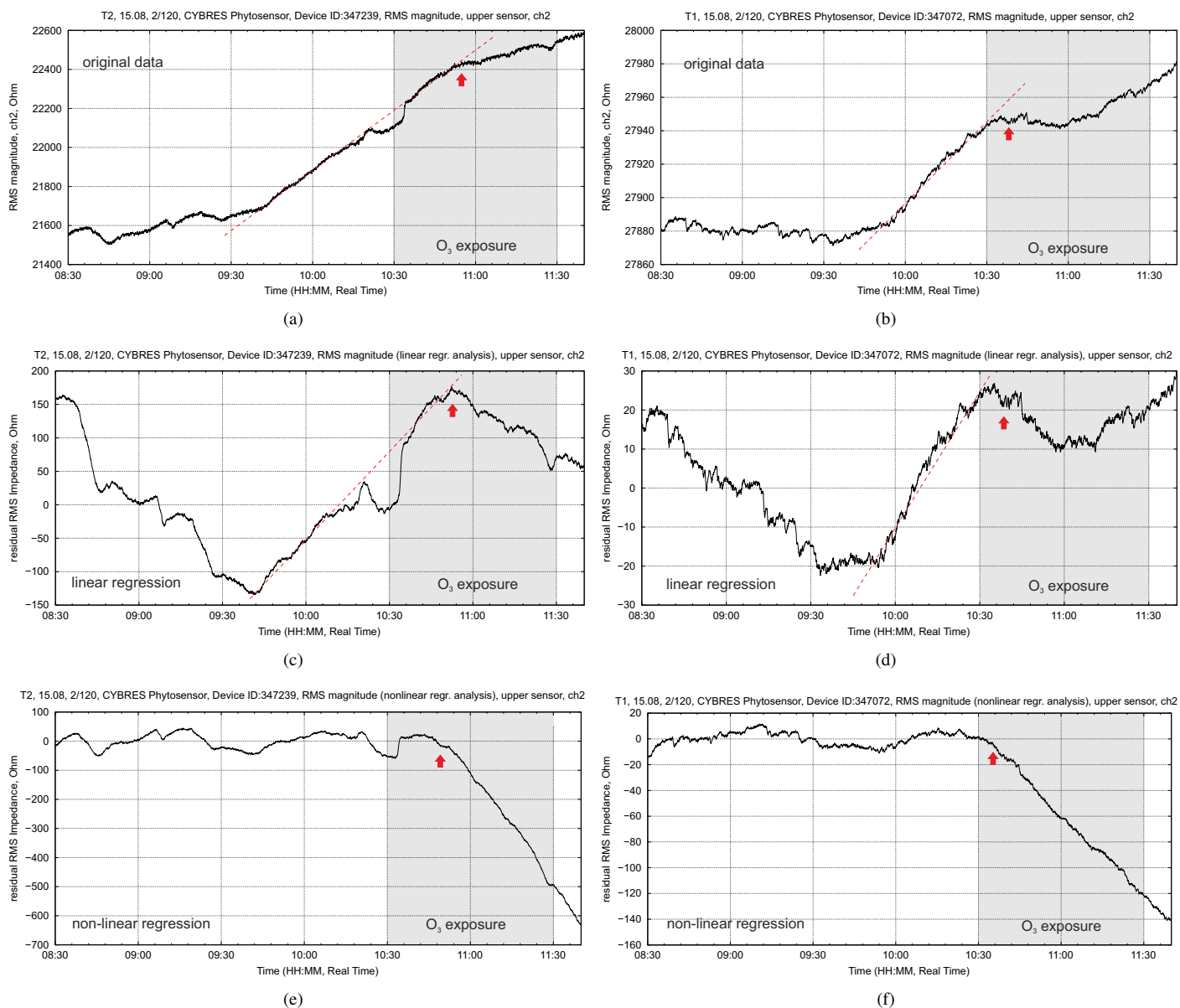


Figure 19. Supplementary image: demonstration of regression analysis for detecting changes of the EIS trend, tobacco T1 and T2 plants, O₃ exposure in 15 ppb range: **(a,b)** Original EIS dynamics of upper sensors; **(c,d)** linear regression up to the inclination point (interpolation after this point); **(e,f)** nonlinear regression with 5th order polynome up to the inclination point (interpolation after this point). In all cases the inclination point is detectable, nonlinear regression provides the best resolution for detection based on $\Psi < 0$ condition, see the expression (3).

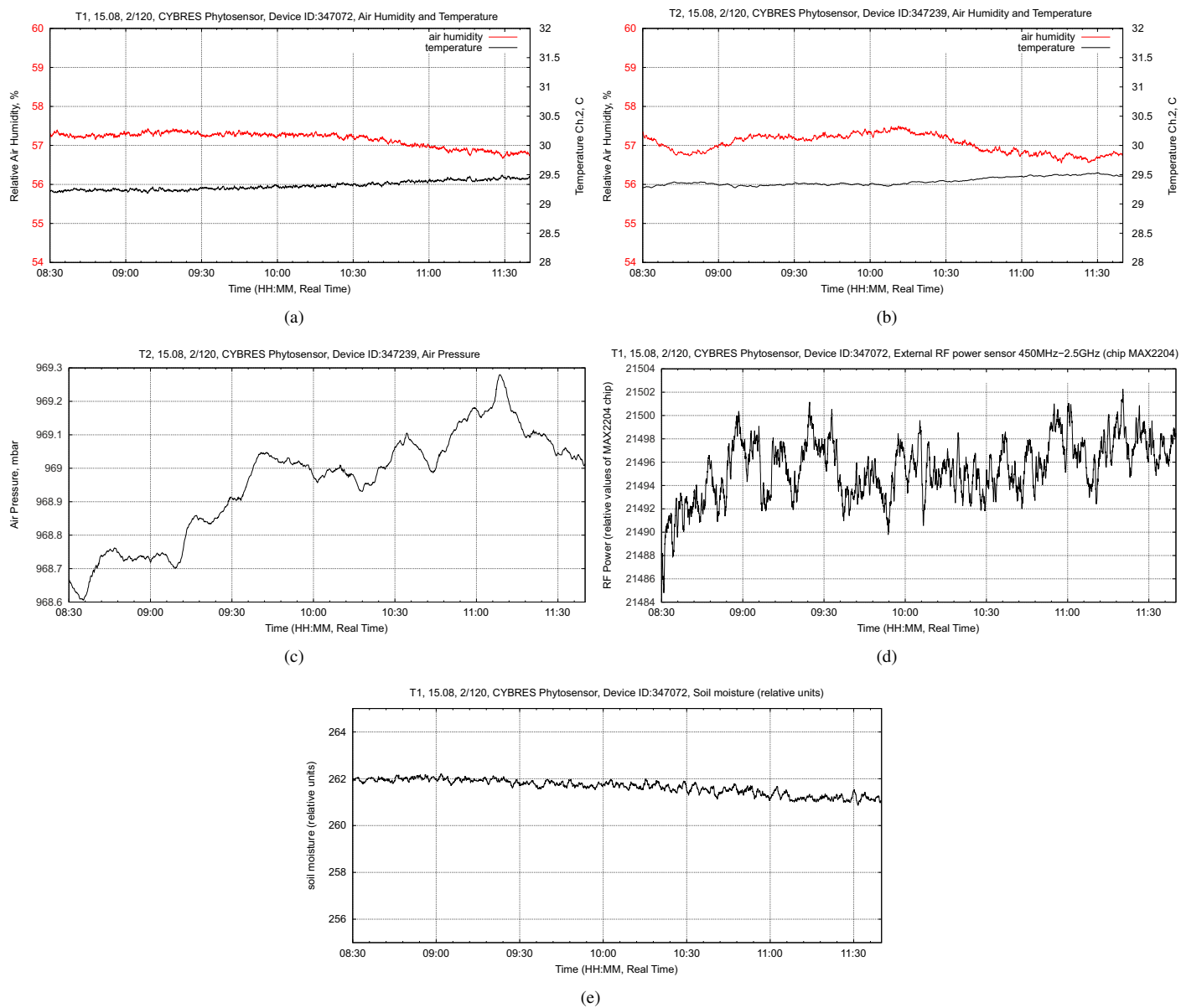


Figure 20. Supplementary image: environmental parameters (air humidity and temperature, atmospheric pressure, EM emission in 450Mhz-2.5Ghz range, soil moisture) for the EIS measurements in Fig. 19 before and during O_3 exposure.

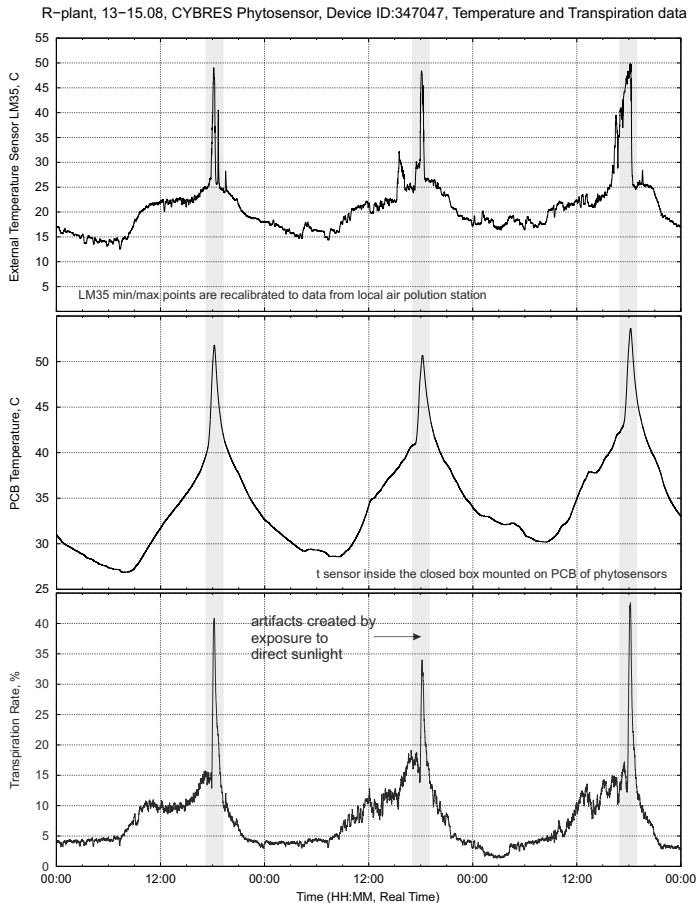


Figure 21. Supplementary image for Fig. 10: environmental temperature (rescaled to data from local air pollution stations), internal temperature of electronic components (inside the closed box) and transpiration in outdoor setup during 72 hours, shadow regions represent a direct sunlight exposure in the afternoon time.

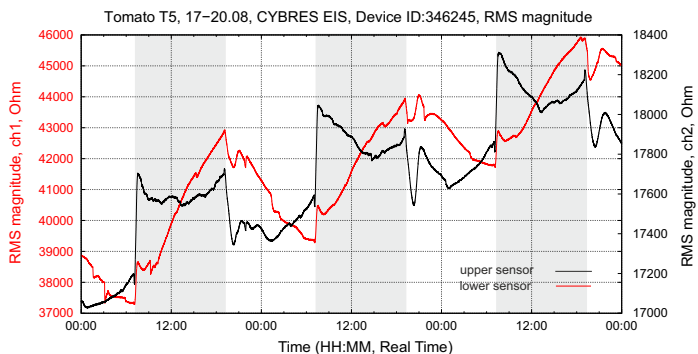


Figure 22. Supplementary image: EIS dynamics of tomato plant (indoor setup) during 72 hours.

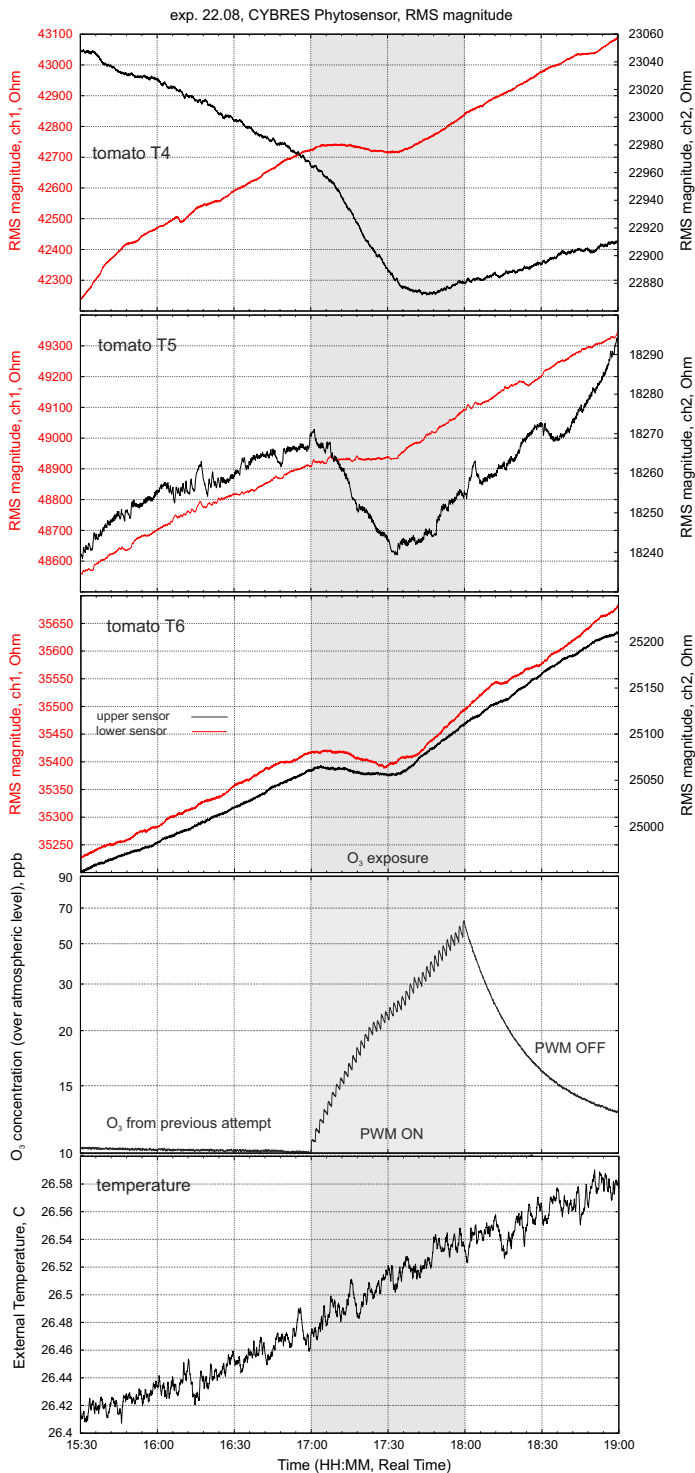


Figure 23. Reaction of three different tomato plants on O₃ exposure (indoor setup), variation of temperature is about 0.2C during 3.5 hours.

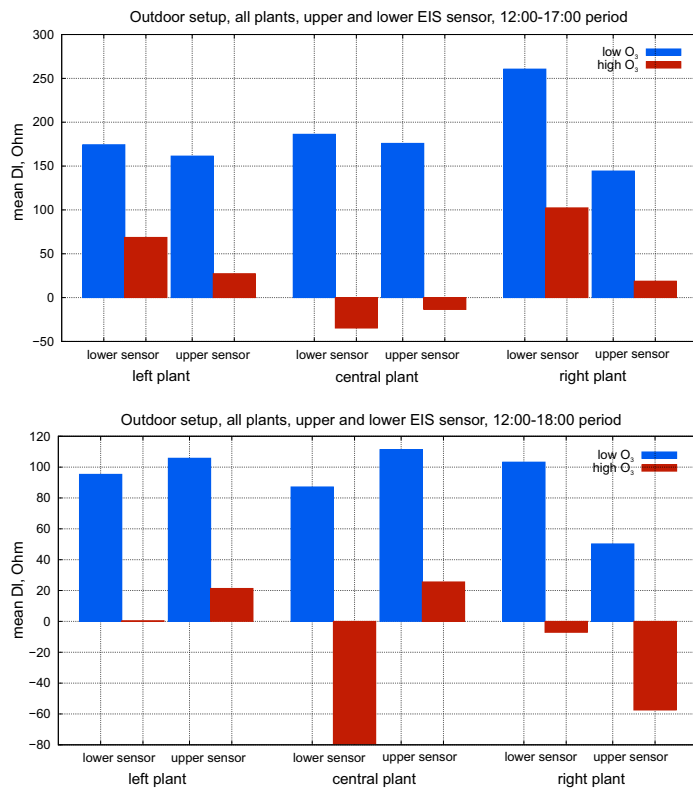


Figure 24. Comparison of means for all sensors and plants for 12:00-17:00 and 12:00-18:00 measurement regions (with heat stress).